Raman Spectroscopy as a Probe of Temperature and Oxidation State for Gadolinium-Doped Ceria Used in Solid Oxide Fuel Cells

R. C. Maher* and L. F. Cohen

The Blackett Laboratory, Prince Consort Road, Imperial College London, London SW7 2BW, United Kingdom

P. Lohsoontorn, D. J. L. Brett, and N. P. Brandon

Department of Earth Science and Engineering, Imperial College London, London, SW7 2BP, United Kingdom

Received: August 8, 2007; In Final Form: December 5, 2007

Raman spectroscopy is a noninvasive and highly sensitive analytical technique capable of identifying chemical compounds in environments that can mimic SOFC operating conditions. Here we demonstrate the use of Raman spectroscopy to perform local thermal and temporal measurements, both of which are essential if phase formation diagrams are to be mapped out and compared to thermodynamic phase stability predictions. We find that the time resolution of the Raman technique is more than sufficient to capture essential dynamic effects associated with a change of chemical composition.

I. Introduction

The solid oxide fuel cell (SOFC) is a solid-state energy conversion device that operates in the range 973−1473 K and shows particular promise for stationary combined heat and power generation applications.[1] Advances have also been made in the development of intermediate temperature (IT) SOFCs operating at a reduced temperature of between 773 and 973 K.[2−4] By lowering the operating temperature, one can use a wider range of materials that allow cost-effective fabrication, particularly in relation to interconnects and balance-of-plant components. There are several potential electrolyte materials with suitable properties for IT-SOFCs.[5,6] Gadolinium-doped ceria (CGO) is a promising candidate that is widely used[7−9] and is used in this demonstration investigation.

Understanding the processes which reduce the efficiency and lifetime of the SOFC is important for developing strategies to minimize their effect. Redox cycling and the formation of secondary compounds are both deleterious to long-term operation. Monitoring the degradation of fuel cell materials is challenging because the high operating temperatures present a challenge for *in situ* study of the reactions and processes occurring within a SOFC during operation. Optical techniques such as IR and Raman spectroscopy are both known to be powerful tools for the study of SOFCs under operational conditions.[10−14] In this paper we show that, as well as being useful to determine local temperature, Raman spectroscopy can also be used to map out the phase stability of the free surface of the anode material *in situ* and at temperature for CGO based materials. These first results are certainly encouraging as they show that the method could be employed widely to understand such issues as carbon poisoning,[15] sulfur poisoning,[12,16,17] or conditions that promote coke formation.[18−20] We show how Raman can be used to probe the electrolyte surface temperature and to monitor the temporal variation of the oxidation state of CGO. Local temperature and local chemical composition information captured at high spatial resolution as a function of variable gas environment and temperature is an encouraging step forward toward better characterization and understanding of these materials. Before presenting these results, we present a short review of how Raman has been applied to the study of SOFCs along with a description of existing ways of mapping temperature distribution in fuel cells and the theory behind using Raman spectroscopy as a temperature probe.

A. Raman Spectroscopy. Raman spectroscopy is a material specific analytical technique that offers sample identification capabilities down to micron spatial resolutions. It is extremely flexible as any excitation wavelength may be used unlike fluorescence and it is noninvasive. The application of Raman to the study of functioning SOFCs is relatively limited and has only been used relatively recently through the pioneering work at the University of Maryland for the study of SOFCs under practical operating conditions, and even then only for high-temperature SOFCs based on YSZ electrolyte.[13,14]

Raman has been applied to the study of many oxide materials which are of interest as possible electrolytes.[21] Many studies have been carried out on doped Ceria nanopowders.[9,22,23] Raman has been shown to be highly sensitive to size and dispersion of the nanoparticles[9,22] as well as to the doping concentration.[23] Raman has also been shown to be a powerful tool in the study of nanograin confinement effects, the effects of local temperature and strain as well as substitutional and nonstoichiometry effects in such samples.[9]

Understanding how these oxides behave under operational conditions is of great importance particularly for the optimization of their performance.[24,25] These materials are exposed to highly reducing atmospheres at high temperatures for prolonged periods of time during operation. Under such conditions the oxides are reduced, depleting their oxygen content leading to a reduction in the ionic conductivity and an increase in the electronic conductivity.[26] Consequently, their efficiency in the SOFC significantly decreases. Previous Raman measurements on YSZ showed that the Raman signal changes significantly upon the reduction of the electrolyte with the change being attributed to an increase in oxygen vacancies.[27]

* Corresponding author. Electronic address: Robert.Maher@imperial.ac.uk.

10.1021/jp076361j CCC: $40.75 © 2008 American Chemical Society
Published on Web 01/29/2008

B. Temperature Measurement. Significant temperature variations occur within SOFCs during their operation which can severely limit their performance and lifetime.[28] As a result, accurate measurement of the temperature distribution within the SOFC system is an important research and diagnostic tool. Temperature is typically measured using thermocouples or thermistors with varying degrees of sophistication. The application of infrared thermal imaging to the study of SOFCs was recently demonstrated.[29] Temperature increases of up to 2.5 K were measured for polarized CGO pellet cells with an accuracy of 0.1 K and a spatial resolution of 0.5 mm. Accurate measurement of absolute temperature is limited for infrared thermal imaging by the need to know the emissivity of the surface. Raman spectroscopy is not constrained in this way and offers a promising alternative means of measuring temperature in operational SOFCs at high spatial resolution.

Both Raman peak position and width are affected by changes in temperature, due to the anharmonic nature of vibrational modes.[30] As a result, the precise peak position or width may be used to estimate the temperature of the surface. Pomfret and co-workers have used the peak position of YSZ as a probe of temperature.[13] Generally, the specific anharmonicity of individual modes will be different and thus the variation of the peak position and width as a function of temperature must be calibrated first. Because of this, care must be taken when comparing Raman measurements of similar samples from different systems, as the experimental conditions of different measurements such as the calibration of the system and the exact temperature of the samples can have significant effects on recorded spectra.

The ratio, ρ, of the intensity of the anti-Stokes to Stokes modes is also extremely sensitive to temperature.[31,32] Under normal nonresonant conditions the intensity of a given Stokes mode, I_S, is dependent on the intensity of the laser, I_L, and the scattering cross-section, σ, of the vibrational mode in question, giving $I_S = \sigma I_L$. The intensity of the anti-Stokes modes I_{aS} is not simply dependent on σ and I_L but also on the vibrational population of the vibrational mode at the time of the measurement. The population of the vibrational mode is given by a Boltzmann distribution, $n = \exp(-\hbar\omega_v/k_BT)$, which is dependent on the temperature of the sample, T, and the energy of the vibration ω_v. $\hbar$ and k_B are the usual constants. As a result $I_{aS} = \sigma I_L \exp(-\hbar\omega_v/k_BT)$. Taking the ratio of I_S and I_{aS} and including the standard wavelength dependence of Raman processes, $(\omega_L + \omega_v)^4/(\omega_L - \omega_v)^4$, gives

$$\rho = (\omega_L + \omega_v)^4/(\omega_L - \omega_v)^4 e^{-\hbar\omega_v/k_BT} \quad (1)$$

It is clear from this equation that low-energy vibrational modes that are close to the laser and have large Raman cross-sections are ideal for the measurement of anti-Stokes/Stokes ratios. It is then trivial to extract the temperature of the sample from such a measurement using eq 1.

II. Experimental Section

Cylindrical electrolyte pellets of yttria-stabilized zirconia (YSZ) were produced by uniaxially pressing YSZ powder (8% mol Y_2O_3, Tosoh, Japan) at 1 tonne for 30 s, followed by sintering at 1723 K in air for 5 h, and pellets of gadolinium doped ceria (CGO) were produced by uniaxially pressing CGO-10 powder ($Ce_{0.9}Gd_{0.1}O_{1.95}$, NextTech Materials) at 1 tonne for 30 s, followed by sintering at 1573 K in air for 5 h. In each case, dense pellets with a calculated density of ~95% were produced that had a thickness of ~1 mm and a diameter of ~12 mm.

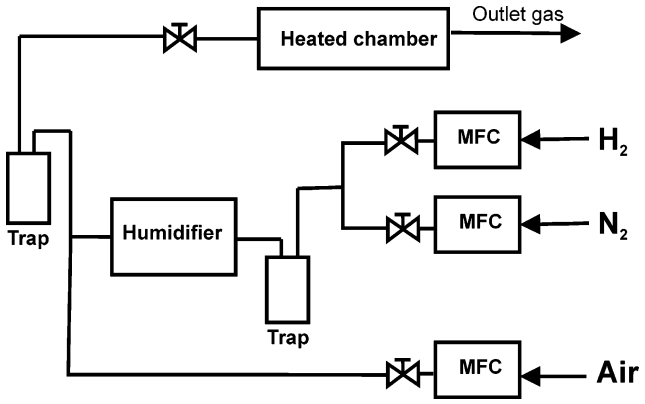

Figure 1. Experimental setup showing the gas supply to the heated stage.

Raman measurements were taken using a Renishaw RM-2000 CCD spectrometer equipped with a Linkam temperature control stage, which allowed the temperature and atmosphere to which the sample is exposed to be controlled. Spectra were obtained using a x50 long working distance objective, which allowed the laser to be focused on to the samples surface to a spot size of approximately 1.5 μm. Measurements were taken using a 633 nm HeNe laser with approximately 5 mW of laser power at the focal point. The integration time was optimized for each sample to give the maximum signal-to-noise ratio possible and will be reported in the description of the individual results. Raman spectra were obtained from the samples between the temperatures of 300 and 873 K as reported by the Linkam stage controller. Spectral features were background corrected and fitted to mixed Gaussian and Lorentzian modes using the Renishaw Wire software. The extracted data were further analyzed using Origin 7.5. The anti-Stokes/Stokes ratio was calculated using the integrated intensity of the Raman modes as both the intensity and line width change with temperature. The system was calibrated before each measurement to the 520 cm^{-1} mode of silicon to make the measurements as consistent as possible. However, the precise position of this mode is dependent on the temperature of the sample when the measurement is made, which may vary slightly from day to day.

Figure 1 shows the test system set up for the delivery of gas to the samples in the furnace. The test system allows different compositions of H_2, N_2, and H_2O to be introduced to the sample. The H_2 and N_2 gas lines (99.99%, BOC, U.K.) connect to calibrated mass flow controllers (Bronkhorst, U.K.) that are available for gas flow rates ranging from 2 to 100 cm^3 min^{-1}. After passing through the mass flow controllers, the H_2 and N_2 lines are combined and the H_2/N_2 line passes through the humidifier, which is a bubble column situated inside a thermocirculator bath, to saturate the gas with water to a level of 3%, giving the requisite gas composition in the heated chamber. A dry air line (BOC, U.K.) is also available and directs to the test chamber. During the measurements, the gas composition was flowed through the cell at a rate of 100 cm^3 min^{-1}.

In studying the CGO sample under reducing conditions, pellets were heated to 873 K in nitrogen (3% H_2O) and allowed to thermalize for 30 min before beginning to flush the stage with 97% H_2 (3% H_2O) at 100 cm^3 min^{-1}. The 460 cm^{-1} CGO peak was monitored continuously as the stage was flushed with H_2 with a 1 s integration time.

III. Results and Discussion

Figure 2 shows the Raman spectra of the (a) YSZ and (b) CGO electrolytes taken using the 633 nm laser with a 1 s

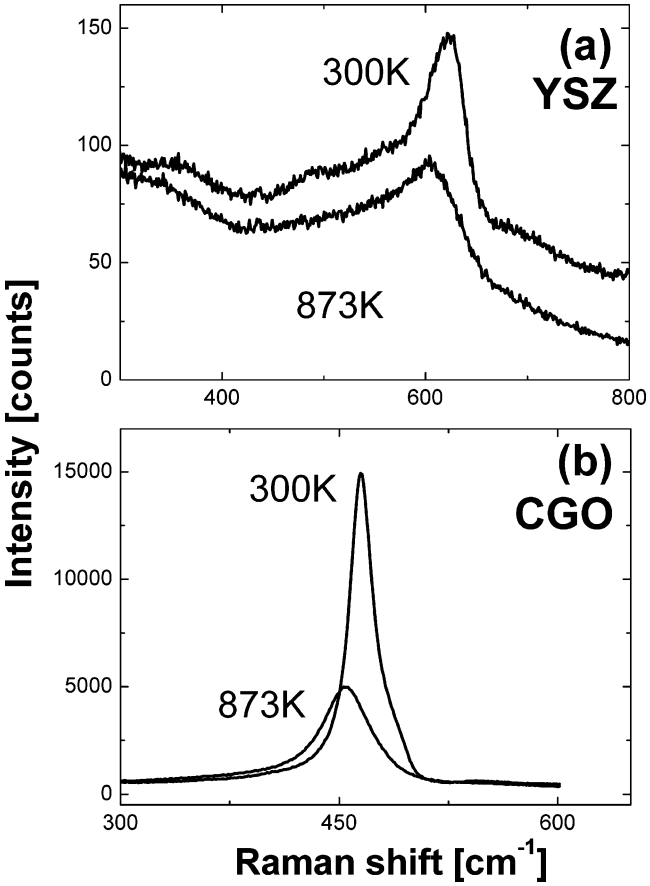

Figure 2. Raman spectra of (a) YSZ and (b) CGO taken using the 633 nm laser at full power and a 10 s integration taken at 300 and 873 K. Note the large difference in intensity between the two spectra and the difference in the spectral range.

integration time at 300 and 873 K. The Raman cross-section of YSZ is clearly much smaller than that of CGO. The spectral features of YSZ are also quite broad making the extraction of temperature information difficult. The spectrum of the CGO sample in contrast is dominated by the well defined, intense F_{2g} Raman peak centered at approximately 460 cm^{-1}. Throughout the rest of this paper, we will refer to this dominant mode of CGO as the 460 cm^{-1} mode, although it will appear at slightly different positions depending on the specific conditions of each measurement.

Temperature information is commonly extracted from Raman spectra using the anti-Stokes/Stokes ratio.[31,32] The 460 cm^{-1} mode of CGO is ideal in this case as it is very intense and relatively close to the laser's frequency, so minimizing the scan time. The sample was heated from 313 to 873 K in air, to ensure the oxidation state of the sample was stable during the measurement. Raman spectra were taken every 5 K using an extended scan from -600 to $+600$ cm^{-1} to include both the anti-Stokes and Stokes modes with an integration time of 30 s. The inset to Figure 3 shows the anti-Stokes/Stokes spectra at high and low temperature. At 300 K the aS signal is small and at high temperature the peaks are highly broadened. Figure 3 shows the anti-Stokes/Stokes ratio calculated from the integrated intensities of the Raman modes for two measurements made on different samples. There are several sources of experimental error. First, the measurements were taken using different samples on different days and the differences between the measurements are due to variations in the quality of the thermal link between the heating element and the sample. Second, it is not usually possible to measure both the anti-Stokes and Stokes modes at

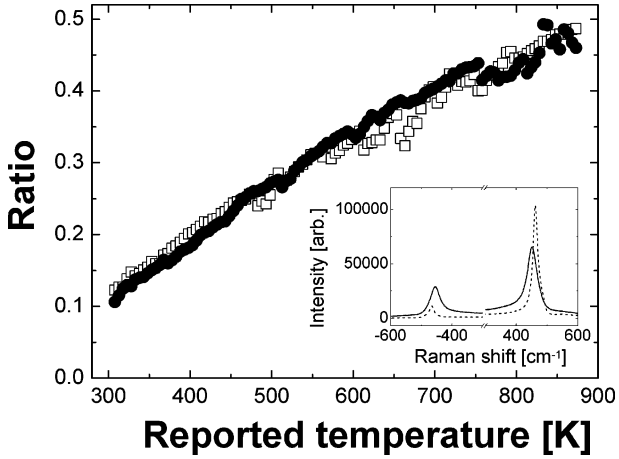

Figure 3. Experimental anti-Stokes/Stokes ratio for the dominant mode of CGO as a function of temperature for two different measurements. (Inset) anti-Stokes and Stokes spectra taken at 313 K (dashed line) and 873 K (solid line).

the same time given the large difference in energy between them as was the case here. The anti-Stokes/Stokes ratio can be significantly affected if the temperature of the sample changes between the measurement of the two modes. One final source of error is introduced by the thermal expansion of the sample as it is heated. The laser must be continuously refocused as a result of thermal expansion changing the collection optics which can introduce artifacts. Such artifacts are visible in the anti-Stokes/Stokes data for both measurements where small steplike features can be observed due to the refocusing. These features are not reproducible and render the aS/S method unusable for temperature calibration purposes. Despite these difficulties it is attractive to think that the anti-Stokes/Stokes ratio could be used to characterize the discrepancies between the reported temperature and the surface temperature resulting from a temperature gradient.

The anti-Stokes/Stokes ratio is not the only property of a Raman spectrum that changes with temperature. The position, width and intensity of the Raman modes will also change. The ability to measure the temperature of a sample based on its Raman features is dependent not only on how well-defined those features are but also on the rate at which that spectral feature changes with temperature. Figure 2 not only shows that the 460 cm^{-1} mode of CGO remains intense as the temperature increases but also shows that there is a strong change in peak position.

Figure 4 shows how the position of the 460 cm^{-1} mode of CGO changes as a function of temperature for the same two measurements shown above in Figure 3. The peak positions start at the same position at low temperature but diverge as the temperature is increased. This is again due to the difference in thermal contact between the samples and heater element. The upper inset shows an expanded view of the range between 775 and 875 K for one of the data sets. Over this range the experimental data are well approximated by a linear fit given by $P = Bx + A$, where P is the position of the Raman peak, B is the rate at which the position of the peak changes with temperature, and A is the position of the peak at 0 K. For this electrolyte material, experiments relevant to fuel cell operation will typically be performed within the temperature range covered in the upper inset of Figure 3.

Clearly the position of the peak varies with temperature far more reliably than the anti-Stokes/Stokes ratio. Several measurements were performed between 773 and 873 K on the same sample to test the reproducibility of the peak shift method when

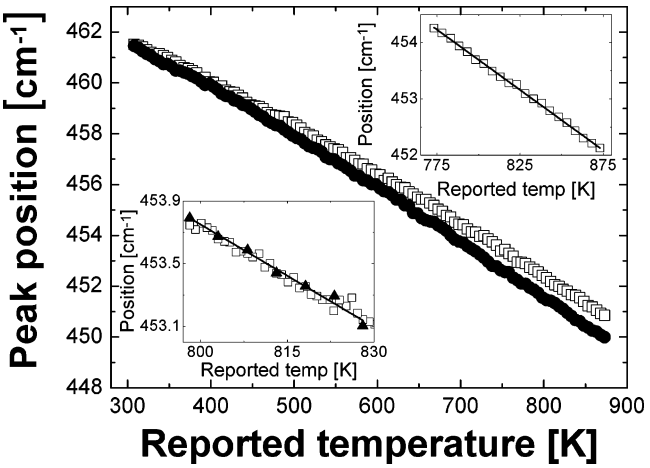

Figure 4. Position of the dominant mode of CGO as a function of temperature. (Top inset) position of the dominant mode of CGO over a restricted range with a linear fit. (Lower inset) repeated temperature ramp measurements of CGO between 795 and 830 K with a 1 K (open squares) and 5 K (solid triangles) resolution on the same sample.

TABLE 1: Values of Different Temperature Ramps Performed between 773 and 873 K, Where *B* Is the Rate at Which the Position of the Peak Changes with Temperature.

ID	*T* (K)	*T* interval (K)	integration (s)	*B*, cm^{-1}/K
1	798−848	1	30	−0.02
2	798−848	1	30	−0.02
3	773−873	5	30	−0.02
4	773−873	5	30	−0.02
5	773−873	5	30	−0.02
6	773−873	5	90	−0.02
7	773−873	5	90	−0.02
8	773−873	5	90	−0.02
9	773−873	5	90	−0.02
10	773−873	5	90	−0.02

the thermal link is unchanged. Most were carried out using a interval of 5 K between measurements but two were carried out with a 1 K interval. The lower inset of Figure 4 shows the position of the 460 cm^{-1} mode as a function of temperature for two measurements carried out on the same sample consecutively, one with a 1 K temperature resolution and the other a 5 K temperature resolution. These two measurements show that the rate of the change of peak position with temperature is reproducible.

Table 1 summarizes the results of two measurements between 798 and 848 K with a resolution of 1 K and eight measurements performed between 773 and 873 K with a resolution of 5 K. The rate of change of the position of the 460 cm^{-1} mode was found to be extremely robust. The accuracy of the temperature extracted from the peak position is directly proportional to the accuracy to which the position of the mode can be determined, which is in turn related to the resolution of the Raman system, how well defined the mode is, and how strongly it depends on temperature. In our case the absolute resolution of the instrument is 0.9 cm^{-1}, which means the absolute temperature value is known within ±22.5 K only. However, the evolution of the peak with temperature is a smooth and well-defined function. The lower inset to Figure 4 shows that we are able to resolve small changed in the peak position (of the order of 0.02 cm^{-1}) that translate to a temperature resolution of the order of 1 K. This means that although the precision of the instrument only allows us to know the absolute temperature to ±22.5 K, we are able to resolve relative changes in temperature to within 1 K as we map across a sample.

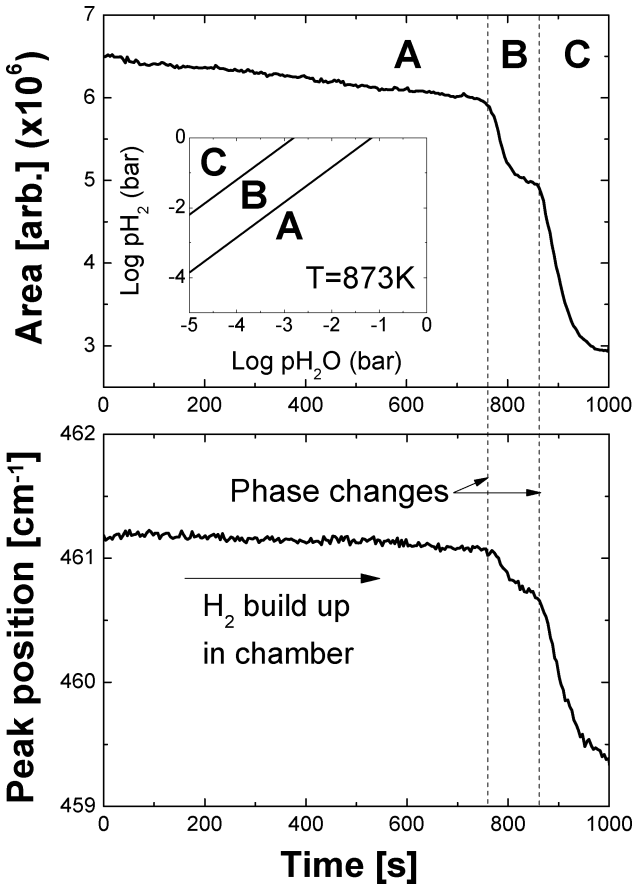

Figure 5. Peak (top) area and (bottom) position of the 460 cm^{-1} mode of CGO as a function of time after beginning to flush the stage with 100% H_2 gas at 873 K. (Top inset) predicted oxidation state of ceria at 873 K as a function pH_2 and pH_2O.

It is clear from these results that Raman is particularly suited to the study of CGO samples at temperatures relevant to IT-SOFC operation and can be used to determine the temperature of the samples surface with a spatial resolution of approximately 1 μm. With our current Renishaw system a temperature resolution of ±2.5 K is attainable (as described using the extrapolation method above); however, with higher resolution systems (with longer focal lengths) this may be improved by at least a factor of 10.

We now turn to the complementary measurements using the Raman technique to probe the oxidation state of the electrolyte. The nonstoichiometry of ceria has been studied extensively and has been found to be a function of the dopant type and concentration, temperature, and gas composition.[33] Ceria can be reduced in the presence of H_2 to give a number of non-stoichiometric forms of CeO_{2-x}, where $1.7 \leq 2 - x \leq 2$.[34,35] Although much work has been done, real time studies of surfaces of electrodes and electrolytes under fuel cell operating conditions is lacking. The inset of the top panel of Figure 5 shows the predicted oxidation state of ceria from thermodynamic phase stability predictions at 873 K as a function pH_2 and pH_2O calculated using HSC Chemistry version 5.1. Although the presence of gadolinium dopant is likely to affect the exact phase properties, the thermodynamic analysis shows that we might expect there to be three possible phases within the realm of the operating conditions imposed on the system, those being: (A) CeO_2, (B) $CeO_{1.85}$, and (C) $CeO_{1.72}$.

To observe the CGO sample under reducing conditions, we first heated it to 873 K in nitrogen (3% H_2O) and allowed it to thermalize for 30 min before beginning to flush the stage with

97% H_2 (3% H_2O) at 100 cm^3 s^{-1}. The 460 cm^{-1} CGO peak was monitored continuously as the stage was flushed with H_2 with a 1 s integration time. Figure 5 shows the peak area and position of the 460 cm^{-1} mode of CGO as a function of time after beginning to flush the stage with an atmosphere of 97% H_2 (3% H_2O). Clearly both the intensity and the position of the CGO 460 cm^{-1} mode are strongly affected by the atmosphere in which it resides and well-defined transitions are observed in the 460 cm^{-1} peak position and area with time exposed to the reducing atmosphere. These changes are reversible on exposure of the samples to air at 873 K on similar timescales. The time scales of the chemical transformations are long compared to the capture data rate, which is governed by the Raman integration time (1 s).

These observations are consistent with those obtained by Pomfret et al. on YSZ in the sense that they observed that the intensity of the Raman modes decreased significantly upon being reduced.[27] They observed a 50% change in the intensity after exposing the YSZ sample to an atmosphere of 5% H_2 95% Ar for 6 h at 1273 K which was reversible upon reoxidation of the sample. Such a reduction in intensity is expected when there is an increased density of oxygen vacancies within the materials leading to a corresponding increase in concentration of cationic metal ion relative to the oxide ions. This results in a decrease in the polarizability and an increase in the surface reflectivity, both of which would result in a decrease in the observed Raman intensity.[36] The thermodynamic calculations show that such a process is expected within the CGO and, supported by the thermodynamic analysis, the three regions shown in Figure 5 are attributed to the three phases of ceria. These results compare well with measurements of the electrical conductivity of cerium dioxide during reduction made by Al-Madfa et al. for which three regions were observed.[26] These first results are certainly encouraging as they show that the real time method, combined with accurate measurement of the surface temperature using the peak position, could be employed widely to understand the dynamics of phase stability and formation of unwanted phase under different experimental conditions highly complementary to thermodynamic calculations.

IV. Conclusion

Raman spectroscopy has previously been shown to be a powerful tool for studying the surface of SOFC electrodes under practical operational conditions such that processes such as coke formation and interaction with sulfur can be studied. The current work focuses on the electrolyte CGO, which is a material used in IT-SOFCs. Exploring both aS/S ratio and peak shift methods to determine surface temperature and relative changes in surface temperature from site to site across a sample, we conclude that it is the peak shift method that is the more reliable, faster, and able to offer higher resolution. These results pave the way for the development of an *in situ* technique capable of mapping temperature distribution at very high spatial resolution in operational SOFCs while simultaneously monitoring chemical composition. Such a facility will be particularly useful for studying very structured and defined electrodes. These two techniques could be compared to thermodynamic calculations to improve the understanding of surface phase stability under experimental conditions pertinent to application.

Acknowledgment. We acknowledge The Ministry of Science and Technology, Royal Thai Government, Thailand, for supporting P.L.'s studentship and the EPSRC SUPERGEN Fuel Cell program for part funding D.J.L.B.

References and Notes

(1) Singhal, S.; Kendall, K. *High-temperature Solid Oxide Fuel Cells: Fundamentals, Design and Applications*, 1st ed.; Elsevier: Oxford, U.K., 2003.
(2) Aguiar, P.; Adjiman, C. S.; Brandon, N. P. *J. Power Sources* **2004**, *138*, 120.
(3) Aguiar, P.; Adjiman, C. S.; Brandon, N. P. *J. Power Sources* **2005**, *147*, 136.
(4) Fergus, J. W. *J. Power Sources* **2006**, *162*, 30.
(5) Goodenough, J. B. *Annu. Rev. Mater. Res.* **2003**, *33*, 91.
(6) Kanou, T. I. F.; Yamasaki, N. J.; Hosoi, S.; Miyazawa, K. T.; Yamada, M.; Komada, N. *J. Alloys Compd.* **2006**, *408*, 512.
(7) Sahibzada, M.; Steele, B. C. H.; Zheng, K.; Rudkin, R. A.; Metcalfe, I. S. *Catal. Today* **1997**, *38*, 459.
(8) Perez-Coll, D.; Nunez, P.; Ruiz-Morales, J. C.; Pena-Martinez, J.; Frade, J. R. *Electrochim. Acta* **2007**, *52*, 2001.
(9) Popovic, Z. V.; Dohcevic-Mitrovic, Z.; Konstantinovic, M. J.; Scepanovic, M. J. *Raman Spectrosc.* **2007**, *38*, 750.
(10) Lu, X.; Faguy, P. W.; Liu, M. J. *Electrochem. Soc.* **2002**, *149*, A1293.
(11) Sum, O. S. N.; Djurado, E.; Pagnier, T.; Rosman, N.; Roux, C.; Siebert, E. *Solid State Ionics* **2005**, *176*, 2599.
(12) Cheng, Z.; Liu, M. *Solid State Ionics* **2007**, *178*, 925.
(13) Pomfret, M.; Owrutsky, J.; Walker, R. *J. Phys. Chem. B* **2006**, *110*, 17305.
(14) Pomfret, M.; Owrutsky, J.; Walker, R. *Anal. Chem.* **2007**, *79*, 2367.
(15) Coutelieris, F. A.; Douvartzides, S.; Tsiakaras, P. *J. Power Sources* **2003**, *123*, 200.
(16) Bartholomew, C.; Agrawal, P.; Katzer, J. *Sulphur Poisoning of Metal, vol. 31 of Advances in Catalysis*, 2nd ed.; Academic Press: New York, 1982.
(17) Hegedus, L.; McCabe, R. *Catalyst Poisoning*; Marcel Dekker: New York, 1984.
(18) Clarke, S. H.; Dicks, A. L.; Pointon, K.; Smith, T. A.; Swann, A. *Catal. Today* **1997**, *38*, 411.
(19) Gupta, G. K.; Hecht, E. S.; Zhu, H. Y.; Dean, A. M.; Kee, R. J. *J. Power Sources* **2006**, *156*, 434.
(20) Liberatori, J. W. C.; Ribeiro, R. U.; Zanchet, D.; Noronha, F. B.; Bueno, J. M. C. *Appl. Catal. A: General* **2007**, *327*, 197.
(21) Gouadec, G.; Colomban, P. J. *Raman Spectrosc.* **2007**, *38*, 598.
(22) Bumajdad, A.; Zaki, M. I.; Eastoe, J.; Pasupulety, L. *Langmuir* **2004**, *20*, 11223.
(23) Dohcevic-Mitrovic, Z. D.; Grujic-Brojcin, M.; Scepanovic, M.; Popovic, Z. V.; Boskovic, S.; Matovic, B.; Zinkevich, M.; Aldinger, F. *J. Phys. Condens. Matter* **2006**, *18*, S2061.
(24) Aneggi, E.; Boaro, M.; de Leitenburg, C.; Dolcetti, G.; Trovarelli, A. *J. Alloys Compd.* **2006**, *408*, 1096.
(25) Chen, H. T.; Choi, Y. M.; Liu, M. L.; Lin, M. C. *Chemphyschem* **2007**, *8*, 849.
(26) Al-Madfa, H. A.; Khader, M. M.; Morris, M. A. *Int. J. Chem. Kinet.* **2004**, *36*, 293.
(27) Pomfret, M. B.; Stoltz, C.; Varughese, B.; Walker, R. A. *Anal. Chem.* **2005**, *77*, 1791.
(28) Apfel, H.; Rzepka, A.; Tu, H.; Stimming, U. *J. Power Sources* **2006**, *154*, 370.
(29) Brett, D.; Aguiar, P.; Clague, R.; Marquis, A.; Schottl, S.; Simpson, R.; Brandon, N. *J. Power Sources* **2007**, *166*, 112.
(30) Ferraro, J. R.; Nakamoto, K. *Introductory Raman Spectroscopy*; Academic Press: San Diego, 1994.
(31) Kip, B.; Meier, R. J. *Appl. Spectrosc.* **1990**, *44*, 707.
(32) Santoro, M.; Lin, J. F.; Mao, H. K.; Hemley, R. J. *J. Chem. Phys.* **2004**, *121*, 2780.
(33) Mogensen, M.; Sammes, N. M.; Tompett, G. A. *Solid State Ionics* **2000**, *129*, 95.
(34) Körner, R.; Ricken, M.; Nötling, J.; Riess, I. *J. Solid State Chem.* **1989**, *78*, 136.
(35) Riess, I.; Ricken, M.; Nölting, J. *J. Solid State Chem.* **1985**, *57*, 314.
(36) Torres, D. I.; Paje, S. E.; Llopis, J.; Morell, G.; Katiyar, R. S. *J. Lumin.* **1997**, *724*, 72−74.